NANO LETTERS

xxxx
Vol. 0, No. 0
A−F

Nanopore Structure and Sorption Properties of Cu–BTC Metal–Organic Framework

Aleksey Vishnyakov,[†] Peter I. Ravikovitch,[†] Alexander V. Neimark,*[,†] Martin Bülow,[‡] and Qing Min Wang[§]

Center for Modeling and Characterization of Nanoporous Materials, TRI/Princeton, 601 Prospect Ave, Princeton, New Jersey 08542, BOC Process Gas Solutions Technology, 100 Mountain Avenue, Murray Hill, New Jersey 07974, and BOC Edwards Corporate Technology Group, 100 Mountain Avenue, Murray Hill, New Jersey 07974

Received March 4, 2003; Revised Manuscript Received April 15, 2003

ABSTRACT

Grand canonical Monte Carlo simulations in conjunction with high-resolution low-pressure argon adsorption experiments were employed to study adsorption mechanisms on the copper(II) benzene-1,3,5-tricarboxylate metal-organic framework (Cu–BTC). We constructed a molecular structural model of Cu–BTC. The pore network of Cu–BTC has a simple cubic symmetry. It consists of main channels of a square cross-section of ca. 0.9 nm diameter and tetrahedral side pockets of ca. 0.5 nm, which are connected to the main channels by triangular windows of ca. 0.35 nm diameter. Using a parameterized united-atom force field, we have determined the preferential adsorption sites and the sequence of adsorption mechanisms from a gradual filling of the side pockets to a stepwise adsorption and condensation in the main channels. The simulation results agree quantitatively with the experimental isotherm of argon up to almost complete filling of the pore network.

Metal-organic frameworks (MOFs, also known as coordination polymers) represent a relatively new family of regular nanoporous materials that are formed by a network of transition metal ions linked by bridging ligands other than oxygen.[1−5] The synthesis of the first MOFs prior to the mid 1990s was driven mostly by topological interest (see ref 1, review ref 2). Several prominent examples were identified; however, their porosity and chemical stability had been limited. Since then, a large number of new coordination polymers with cationic, anionic, and neutral frameworks have been synthesized (see, e.g., refs 2−7). Some of the recently synthesized MOFs possess high microporosity and considerable chemical stability. Due to a finely controlled pore structure, functionalized MOFs are likely to have considerable advantages over other microporous materials such as zeolites and microporous carbons, which are currently utilized for adsorption separations, catalysis, and gas storage.[2] Coordination chemistry of metal ions has been thoroughly studied; it is discussed in the literature whether the engineering of new MOFs is synonymous with the crystal structure prediction.[8] Since reactions of MOF assembly proceed commonly in solution at room temperature, synthesis of a MOF with desired pore structures, functionalities, and sorption properties may be easier than that, for example, of a novel zeolite. MOFs may provide new opportunities for practical applications due to specific properties of their networks such as flexibility[9] and chirality.[10,11] The latter arises from enantiomeric ligands and/or an asymmetric framework topology.

Despite an abundance of newly synthesized structures, the adsorption properties of MOFs and, most importantly, the underlying adsorption mechanisms are poorly understood. The pore filling occurs at very low gas pressures, and high-quality adsorption studies of MOF are almost lacking. Experiments on adsorption separation on MOF are quite scarce.[13,14]

In the present work, we study adsorption properties of a MOF by the means of Monte Carlo (MC) simulations combined with high-resolution, low-pressure adsorption experiments. As an instructive example, we investigate Ar adsorption on copper(II) benzene-1,3,5-tricarboxylate, Cu−BTC. Cu−BTC is a neutral coordination polymer composed of dimeric cupric tetracarboxylate units[3] (Figure 1). Twelve carboxylate oxygen atoms from the two BTC ligands bind to four coordination sites for each of the three Cu^{2+} ions. These copper−benzenecarboxylate units form a face-centered crystal lattice of $Fm3m$ symmetry, which has a complex three-dimensional channel system as depicted in Figure 2. The main pores of ca. 0.9 nm in diameter form a cubic

* Corresponding author. E-mail: aneimark@triprinceton.org
† TRI/Princeton.
‡ BOC Process Gas Solutions Technology.
§ BOC Edwards Technology.

10.1021/nl0341281 CCC: $25.00
Published on Web 00/00/0000

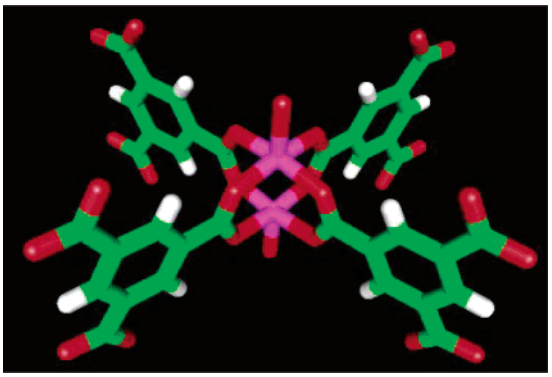

Figure 1. Dicopper tetracarboxylate building block for CuBTC. Cu−Cu distance is 0.2628 nm Cu−O 0.1952 nm[3]. Copper in violet, carbon in green, hydrogen in white, oxygen in red.

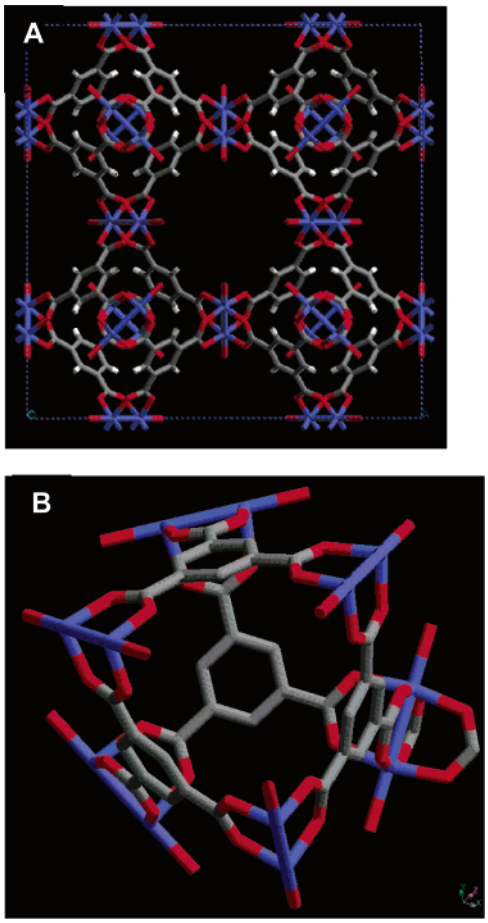

Figure 2. Pore network of Cu−BTC. (A) View from [100] direction. Roughly rectangular pores of ca. 0.9 nm in width form a 3D cubic network. (B) View from a direction close to [111] shows the tetrahedron-shaped side pockets with triangular windows of internal diameter of 0.35 nm. The windows of the pockets are open to the main channels.

network that is well seen from the [100] direction (Figure 2a). In addition, planar $C_3H_6(O_2C)_3$ segments form tetrahedron-shaped side pockets (Figure 2b). The window of these pockets is ca. 0.35 nm in diameter (Figure 2b), which is wide enough for small molecules of gases to pass through, but it is too tight for larger organic molecules. When exposed to water, Cu−BTC forms a crystallohydrate, $[Cu_3(BTC)_2(H_2O)_3]_n$, which has a light blue color, while dry Cu−BTC is dark purple.[13]

We synthesized Cu−BTC using an improved technique that targeted large-scale industrial production.[13] The technique consists of hydrothermal formation of Cu−BTC at 383 K (or 423 K) from a premixed ethanolic aqueous solution (1:1 vol) that contains benzene-1,3,5-tricarboxylic acid and cupric nitrate over a period of 18 h (details are given in the Appendix). The XRD, elemental, and ICP analyses, and TGA measurements identified the product to be the same as the original structure discovered by Chui et al.[3]

Argon adsorption isotherm measurements were performed on dry Cu−BTC at the boiling temperature of Ar, 87.3K (details are given in Appendix). Low-temperature Ar adsorption is known to be a very sensitive test of subtle structural features of crystalline microporous materials. It provides indispensable experimental information for a justification of the potential models used in molecular simulations.[15] The isotherm is presented in Figure 3. High-resolution measurements at extremely low pressures allowed us to obtain a linear interval of the adsorption isotherm at vapor pressures, $p < 7\times10^{-6}$ atm. In this low-pressure region, adsorbate−adsorbate interactions are negligible, and the Henry law (upper inset in Figure 3) describes adsorption fairly well. The Henry constant is a very important parameter for validation of the force field for MC simulations.[16,17] At higher pressures, the isotherm exhibits a plateau at $7.3\times10^{-5} < p < 4.0\times10^{-4}$ atm, which is followed by a near-vertical step at $p \approx 7.0\times10^{-4}$ atm. After the step at $8\times10^{-4} < p < 1$, adsorption increases continuously to 13.2 mmol/g. A small hysteresis at $p > 0.40$ atm indicates mesoporosity originated most probably from intercrystalline voids in the sample. From the experimental isotherm, the micropore volume of Cu−BTC is estimated as 0.34 cm^3/g or 40% of the unit cell volume; the total pore volume is estimated as 0.37 cm^3/g; the surface area is estimated as ~1500 m^2/g. Note, that the porosity of Cu−BTC is very high for a crystalline material. It is about one-and-a-half two times higher than the porosity of conventionally used zeolites, such as ZSM-5 (~0.18 cm^3/g), NaX, and NaY (~0.3 cm^3/g).

The core problem in molecular simulations consists of a reliable force field capable of accounting for interatomic and intermolecular interactions with minimum input parameters. So far, no potential model suitable for molecular simulations of gas adsorption on Cu−BTC has been reported. In simulations of adsorption by zeolites, interactions of adsorbing species with the zeolite framework oxygen atoms effectively describe the adsorption potential; their interactions with silicon atoms and metal ions are neglected. However, it was difficult to simulate low-temperature isotherms on zeolites, which possess a complex pore structure with connecting pores and side pockets, even for simple gases such as nitrogen and argon.[15] More sophisticated models account for flexibility of the zeolite lattice and consider the motions of ions that occur in conjunction with the adsorption process.[18]

We attempted to reproduce the experimental Ar adsorption isotherm on Cu−BTC in Monte Carlo simulations (details

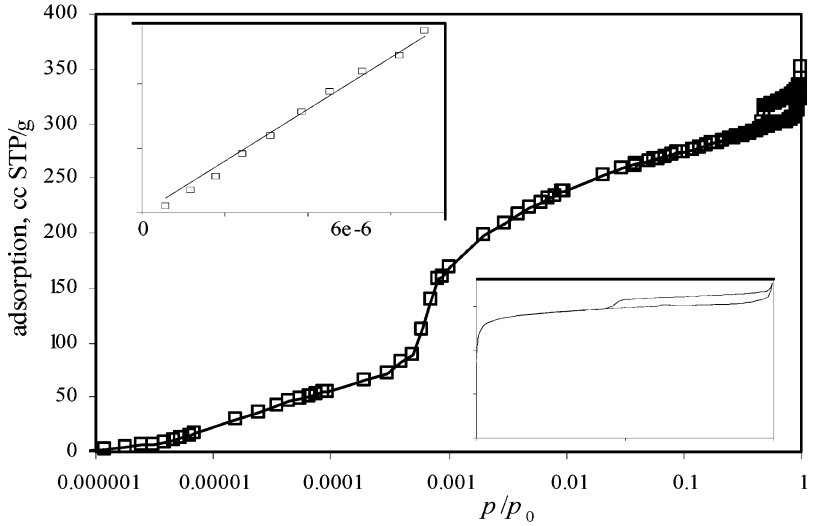

Figure 3. Experimental Ar adsorption isotherm on Cu−BTC at 87.3 K. The inset in the lower right corner shows the isotherm in the linear pressure scale. The inset in the upper left corner shows the same isotherm in the low-pressure region.

Table 1. Lennard-Jones Parameters of Intermolecular Interaction of the Cu−BTC Lattice with Argon

parameter		force field (i)	(ii)	(iii)	(iv)
Ar−Ar	σ, nm	0.344	0.340	0.340	0.340
	ϵ/k, K	93.27	119.8	119.8	119.8
Cu−Ar	σ, nm	0.2984	0.2984	0.2984	0.296
	ϵ/k, K	26.56	26.56	26.56	25.6
O−Ar	σ, mn	0.328	0.318	0.320	0.32
	ϵ/k, K	53.12	112.6	101.3	86.13
$C_{benzene}$−Ar	σ, nm	0.344	0.3475	0.364	0.364
	ϵ/k, K	70.27	65.03	50.15	42.63
$CH_{benzene}$−Ar	σ, nm	0.344	0.3475	0.3547	0.3545
	ϵ/k, K	70.27	65.03	57.39	65.78
$C_{carboxyl}$−Ar	σ, nm	0.344	0.3575	0.3575	0.3575
	ϵ/k, K	70.27	79.64	79.64	67.7
H−Ar	σ, nm	0.301	0.291		
	ϵ/k, K	45.49	42.57		

are given in Appendix). For this purpose, a structural model of Cu−BTC was constructed from XRD data given in ref 3 using the Cerius2 crystal builder.[19] The atoms of the crystal lattice were assumed to be immobile. To represent the interactions of the atoms of the solid with Ar, we employed four different force fields (FF).

(i) *All-atom universal force field (UFF) of Rappe et al.*[20] The parameters of UFF were fitted to the results of ab initio calculations of organic molecules of different classes; nonbonded interactions are commonly represented by 12−6 Lennard-Jones (LJ) potentials, which are assigned to each type of atoms. The parameters for interatomic LJ interactions are calculated from the individual LJ parameters by using the Lorentz−Berthelot (LB) combination rules, $\epsilon_{ij} = \xi(\epsilon_{ii}\epsilon_{jj})^{1/2}$ and $\sigma_{ij} = \chi(\sigma_{ii} + \sigma_{jj})/2$ with $\xi = \chi = 1$. The parameters employed are given in Table 1. Note that the LJ model of Ar in UFF underestimates the critical temperature of pure Ar by 33 K (as calculated using the equation of Johnson et al. for LJ fluid[21]). Correspondingly, the saturated vapor pressure at 87.3 K is close to 5 atm, which influences the shape of the simulated isotherm.

(ii) *All-atom OPLS force field.*[22] With this model, we used established Ar−Ar LJ parameters;[23] however, the cutoff radius was 5σ. This model of Ar was employed in previous works;[24,25] it represents very accurately (within 1−2%) the experimental vapor−liquid diagram of bulk Ar (calculations were performed using the equation of state of Johnson et al.[21]). The parameters for oxygen atoms were equal to the LJ parameters of carboxyl oxygen. LB combination rules with $\xi = \chi = 1$ were used. The Cu−Ar parameters were taken from UFF.[20]

(iii) *United-atom force field with C−H benzene group represented as one LJ site*.[26] This FF was compiled from several different sources (Table 1). The same Ar model as in (ii)[24] was used, and LB combination rules with $\xi = \chi = 1$ were used in these simulations. The Cu−Ar parameters were taken from UFF.[20]

(iv) *The same force field as (iii) with LB coefficients ξ and χ modified to reproduce in simulations the experimental Henry constant*. In all simulations, the electrostatic potential was neglected.

Static energy optimization proves that the side pockets are preferential adsorption sites for Ar in the Cu−BTC lattice (Figure 4). The adsorption potential in the side pockets is as deep as 14.5 kJ/mol. In the center of the intersection of the main channels, the solid-fluid energy has a maximum at 2.4 kJ/mol. For comparison, the potential depth of Ar on the base plane of graphite is about 8.96 kJ/mol, according to the standard LJ model.[24]

The simulated adsorption isotherms obtained with different force field expressions are shown in Figure 5. All isotherms reproduce qualitatively a plateau after the Henry region, which is followed by a near-vertical step. After the step, there is another plateau. The second plateau is followed by another step that is not observed experimentally. All force fields overestimate substantially the adsorption capacity of Cu−BTC for Ar at 87.3 K.

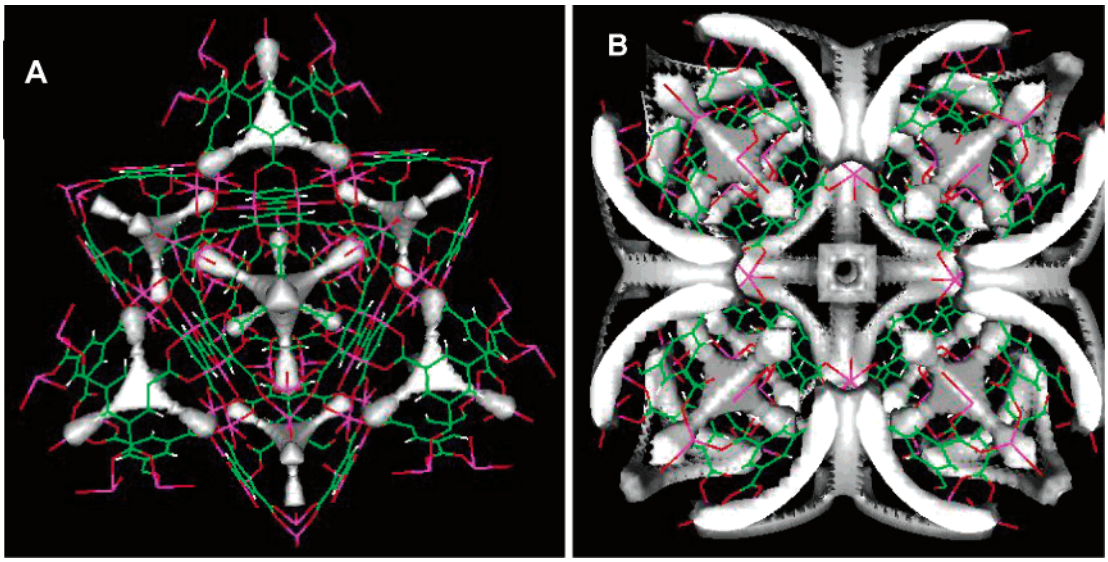

Figure 4. Potential map of Ar in Cu−BTC framework. The deepest minima of 14.5 kJ/mol correspond to the tetrahedron-shaped pockets. The maxima of the solid-fluid potential correspond to the intersection of the main channels. White clouds show the regions with the adsorption potential deeper then 10 kJ/mol (panel A) and 7 kJ/mol (panel B). In Cu−BTC frameworks, copper is shown in violet, carbon in green, oxygen in red, and hydrogen in white.

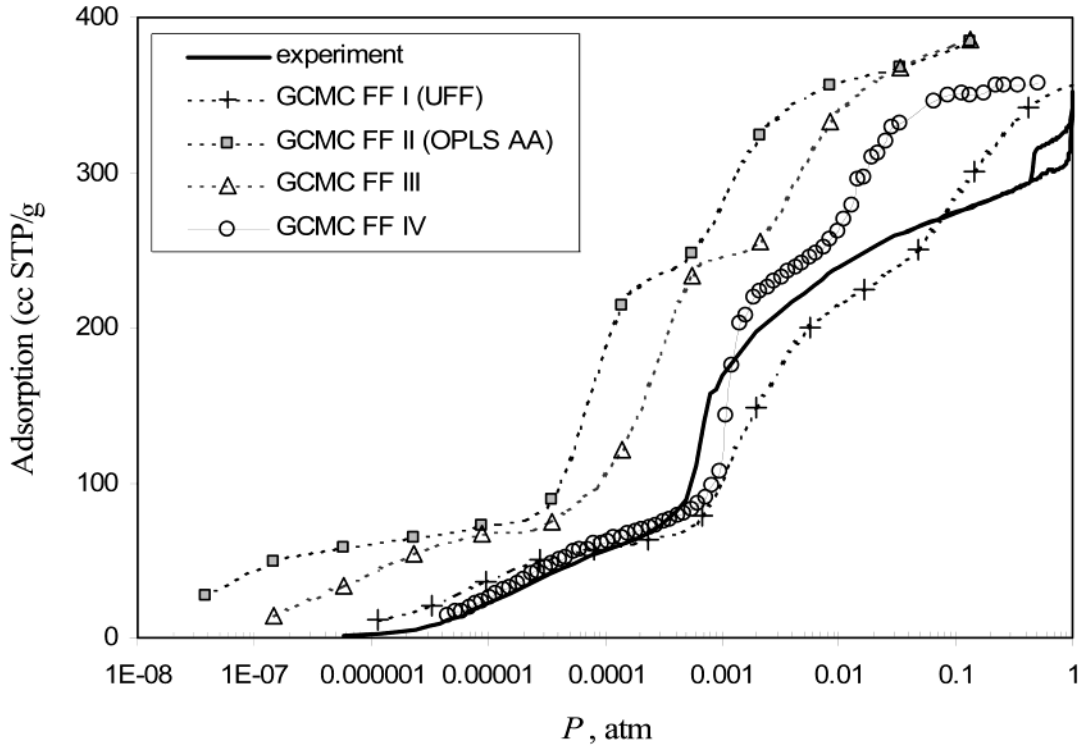

Figure 5. Experimental and simulated Ar sorption isotherms for Cu−BTC at 87.3 K obtained with different force fields. All simulated isotherms represent qualitatively the two step-like features on the experimental one: the steps correspond to filling of the side pockets and main channels. However, the simulations overestimate the adsorption capacity at higher pressures. Only force field (iv), which is validated against experimental vapor−liquid phase diagram for bulk Ar and the experimental Henry constant, is capable of reproducing quantitatively the experimental isotherm below 0.01 atm.

To interpret the simulated isotherms, we employed snapshots and three-dimensional local-density profiles of Ar in the Cu−BTC lattice. Characteristic snapshots are shown in Figure 6. Before the first step occurs, the adsorbate occupies the tetrahedral pockets. Each pocket may accept only one Ar molecule, and four other Ar molecules can be placed at the outer side of the windows. Their positions are close to those of the imaginary vertices of the tetrahedron formed by the planes of benzene rings (Figure 6a). In the experiment, the transfer of molecules into the side pockets can occur only through the windows. Thus, adsorption of larger molecules in side pockets may be blocked, which would cause a disagreement with GCMC simulations, where the molecules are inserted into and removed from the lattice in a random

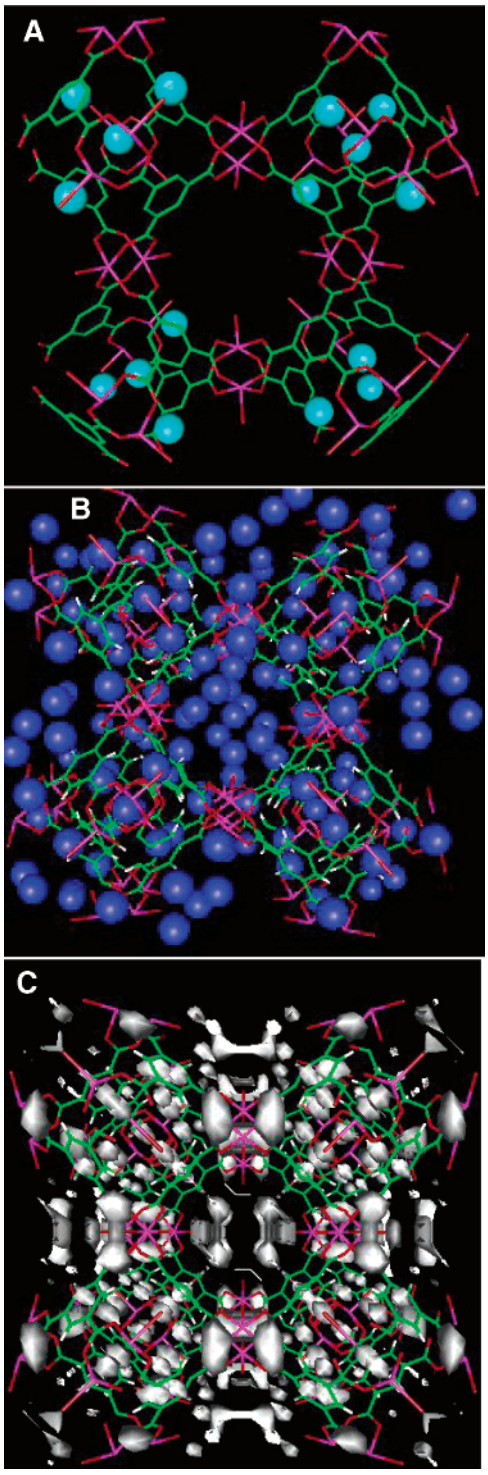

Figure 6. Snapshots of the molecular configurations of Ar in Cu−BTC lattice at $p = 0.0001$ atm (panel A) and $p = 0.01$ atm (panel B) at 87.3 K. At $p = 0.0001$ atm, Ar molecules occupy the tetrahedral pockets and the outer sides of the windows between the pockets and the main pore. At $p = 0.01$ atm, all pores are filled by the adsorbate. Panel C shows 3D local-density profiles of Ar at $p = 0.1$ atm: white clouds show the regions where the local average density of Ar exceeds 40 mol/L (the density of liquid Ar at 87.3 K is ~34.9 mol/L). The adsorbate is highly structured: practically, every molecule has an exact position. Copper in violet, oxygen in red, carbon in green, argon in blu; hydrogen is omitted.

manner. In the case of Ar, the side pockets are accessible, which is confirmed by the fact that the experimental adsorption isotherm is nicely reproduced in GCMC simulations.

Comparing the results of simulations and experiments, we conclude that the step in the experimental adsorption isotherm corresponds to the filling of the main channels (Figure 6b). GCMC simulations with force field (iv) reproduce the location of the step and the plateau region following the step quite reasonably. Although at $p = 0.01$ atm, where all pores in the lattice seem to be filled, the GCMC simulations predict a second step on the isotherm at $p \approx 0.03$ atm. An analysis of adsorbate configurations shows that this step reflects a freezing transition, which is accompanied by a density alteration and molecular ordering. Local-density profiles (Figure 6c) show that every Ar atom has almost an exact position in the lattice, in contrast to the configurations generated at $p < 0.02$ atm. It is difficult to judge why the freezing transition is not observed experimentally. It may be an artifact of simulations since the models employed here do not account for the network flexibility.

It should be noted that force field (iv), which is based on the experimental Ar vapor−liquid diagram and the Henry constant, is able to describe quantitatively Ar adsorption by Cu−BTC at $p < 0.01$ atm. The generic force field expressions (i−iii) overestimate the Henry constant; force fields (ii) and (iii) underestimate severely (more than by 1 order of magnitude) the filling pressure of the main channels. On the other hand, the UFF force field, which also overestimates the Henry constant, predicts reasonably well the filling pressure but shows afterward a gradual increase of adsorption because of incorrect fluid-fluid parameters.

Using the force field (iv) parameters, we predicted the Ar adsorption on Cu−BTC at 296 K. The isotherm was practically linear up to ca. 8 atm with the Henry constant of 0.14 mmol/g/atm. This value is of the same order as in recent simulations of Ar in silicalite (0.175 mmol/g/atm).[27] The total adsorption capacity of Cu−BTC at 8 atm is slightly higher than that for silicalite.[28]

In conclusion, we have studied the mechanisms of Ar adsorption in the pore network of Cu−BTC, i.e., copper(II) benzene-1,3,5-tricarboxylate coordination polymer in its pore network. A combination of MC molecular simulations and high-resolution low-pressure adsorption experiments allowed us to identify the adsorption sites and the sequence of pore filling. The pore structure consists of the main channels, which have a square cross-section and form a cubic network, and the tetrahedron-shaped side pockets. The side pockets are shown to be preferential sorption sites for Ar molecules. They are filled prior to the main channels. Based on the experimental phase diagram for bulk Ar and the Henry region of the experimental isotherm, we have verified a set of parameters for a simple united-atom force field. MC simulations with this force field reproduced quantitatively the experimental isotherm at vapor pressures below 0.01 atm, up to a near-complete filling of the pores in Cu−BTC.

Appendix. Experimental and Simulation Procedures. *Synthesis of Cu−BTC.* Benzene-1,3,5-tricarboxylic acid (49.1 g, 0.234 mol) was dissolved in ethanol (250 mL), and cupric nitrate hydrate ($Cu(NO_3)_2 \cdot 2.5H_2O$; 108.6 g, 0.466 mol) was

dissolved in water (250 mL). The two solutions were mixed at ambient temperature for 30 min, and the mixture was transferred into an autoclave. The autoclave was heated at 383 K (or 423 K) under hydrothermal conditions for 18 h. The reaction vessel was cooled to ambient temperature, and blue crystals of Cu−BTC were isolated by filtration and washed with water. The product was dried overnight at 383 K. The yield was quantitative (80 g). A synthesis procedure scaled-up to pilot-plant batch size has been envisioned. The product was characterized by (i) elemental analysis calculated for $Cu_3(BTC)_2(H_2O)_4$ (wt. %): ideal C 31.94; H, 2.08; Cu, 28.16. Found C, 31.84; H, 1.94; Cu, 28.75; (ii) ICP analysis: CuO, 35.7 wt. %; (iii) loss on ignition: 65.5%; (iv) TGA analysis: the fully hydrated product contains up to 40 wt. % water and is stable up to a temperature of about 673 K.

Adsorption Measurements. The argon adsorption isotherm was measured volumetrically at 87.3 K (liquid Ar temperature) up to atmospheric pressure using an automated adsorption instrument Autosorb 1-C (Quantachrome Corp.) equipped with a MKS Baratron pressure transducer (pressure range: 1×10^{-4}−1 Torr). Before the measurements, a sample (ca. 0.03 g) was outgassed at 473 K over a period of 18 h. Determination of the void volume was performed using helium. Corrections on the thermal transpiration effect were applied according to the standard procedure. A total of 161 adsorption and desorption points were collected over a period of 110 hours. It took ca. 50 h to acquire the data points below the pore filling step (below 0.001 atm), and another ca. 50 h to reach the saturation pressure.

Monte Carlo Simulations. GCMC simulations were performed using the standard algorithms[29] with no configurational bias. The program for MC simulations of adsorption on rigid pore structures was developed at TRI/Princeton. The program was verified with simulation of the adsorption isotherm of methane on silicalite-I at 298 K, which was thoroughly studied previously by experiments and simulations.[30−32] The simulation cell was cubic, 2.6344 nm in size. It was composed of eight elementary cells of the Cu−BTC crystal lattice. Periodic boundary conditions were applied in all three dimensions. A typical length of GCMC simulation comprised 3×10^7 steps (each step consisted of successive attempts of molecule displacement, insertion, and removal), the fluid properties were averaged over 3×10^7 steps. The crystal and local fluid densities were visualized using Cerius2 (version 4.2)[19] and gOpenMol 2.0[33] software.

References

(1) Abrahams, B. F.; Hoskins, B. F.; Liu, J.; Robson, R. *J. Am. Chem. Soc.* **1991**, *113*, 3045.
(2) Barton, T. J.; Bull, L. M.; Klemperer, W. G.; Loy, D. A.; McEnaney, B.; Misono, M.; Monson, P. A.; Pez, G.; Scherer, G. W.; Vartuli, J. C.; Yaghi, O. M. *Chem. Mater.* **1999**, *11*, 2633.
(3) Chui, S. S. Y.; Lo, S.; Charmant, J. P. H.; Orpen, A. G.; Williams, I. D. *Science* **1999**, *283*, 1148.
(4) Eddaoudi, M.; Kim, J.; O'Keeffe, M.; Yaghi, O. M. *J. Am. Chem. Soc.* **2002**, *124*, 376.
(5) Li, H.; Eddaoudi, M.; O'Keeffe, M.; Yaghi, O. M. *Nature* **1999**, *402*, 276.
(6) Nori, S.; Kitagawa, S.; Kondo, M.; Seki, K. *Angew. Chem., Intl. Ed. Engl.* **2000**, *39*, 2082.
(7) Batten, R. S.; Robson, R. *Angew. Chem., Int. Ed. Engl.* **1998**, *37*, 1460.
(8) Zaworotko, M., J. *Angew. Chem., Int. Ed. Engl.* **2000**, *39*, 3052.
(9) Cussen, E. J.; Claridge, J. B.; Rosseinsky, M. J.; Kepert, C. J. *J. Am. Chem. Soc.* **2002**, *124*, 9574.
(10) Hong, M.; Dong, G.; Duan, C. Y.; Li, Y. T.; Meng, Q. J. *J. Chem. Soc., Dalton Trans.* **2002**, 3422.
(11) Kepert, C. J.; Prior, T. J.; Rosseinsky, M. J. *J. Am. Chem. Soc.* **2000**, *122*, 5158.
(12) Fletcher, A. J.; Cussen, E. J.; Prior, T. J.; Rosseinsky, M. J.; Kepert, C. J.; Thomas, K. M. *J. Am. Chem. Soc.* **2001**, *123*, 10001.
(13) Wang, Q. M.; Shen, D.; Bulow, M.; Lau, M. L.; Deng, S.; Fitch, F. R.; Lemcoff, N. O.; Semanscin, J. *Microporous Mesoporous Mater.* **2002**, *55*, 217−230.
(14) Onishi, S.; Ohmori, T.; Ohkubo, T.; Noguchi, H.; Di, L.; Hanzawa, Y.; Kanoh, H.; Kaneko, K. *Appl. Surf. Sci.* **2002**, *196*, 81.
(15) Macedonia, M. D.; Moore, D. D.; Maginn, E. J.; Olken, M. M. *Langmuir* **2000**, *16*, 3823.
(16) Ravikovitch, P. I.; Vishnyakov, A.; Russo, R.; Neimark, A. V. *Langmuir* **2000**, *16*, 2311.
(17) Ravikovitch, P. I.; Vishnyakov, A.; Neimark, A. V. *Phys. Rev. E* **2001**, *6401*, 1602.
(18) Buttefey, S.; Boutin, A.; Fuchs, A. H. *Mol. Simul.* **2002**, *28*, 1049.
(19) Accelrys, Inc. *Cerius2*, 4.2 ed.; Accelrys Inc: San Diego, CA, 2000.
(20) Rappe, A. K.; Casewit, C. J.; Colwell, K. S.; Goddard, W. A.; Skiff, W. M. *J. Am. Chem. Soc.* **1992**, *114*, 10024.
(21) Johnson, J. K.; Zollweg, J. A.; Gubbins, K. E. *Mol. Phys.* **1993**, *78*, 591.
(22) Jorgensen, W. L.; Maxwell, D. S.; Tirado-Rives, J. *J. Am. Chem. Soc.* **1996**, *118*, 11225.
(23) Hirschfelder, J. O.; Curtiss, C. F.; Bird, R. B. *Molecular Theory of Gases and Liquids*; Wiley & Sons: New York, 1954.
(24) Vishnyakov, A.; Neimark, A. V. *J. Phys. Chem. B* **2001**, *105*, 7009.
(25) Neimark, A. V.; Ravikovitch, P. I.; Vishnyakov, A. *J. Phys. Condes. Matter* **2003**, *15*, 347.
(26) Wick, C. D.; Martin, M. G.; Siepmann, J. I.; Schure, M. R. *Int. J. Thermophys.* **2001**, *22*, 111.
(27) Talu, O.; Myers, A. L. *Colloid Surf., A* **2001**, *187*, 83.
(28) Skoulidas, A. I.; Sholl, D. S. *J. Phys. Chem. B* **2002**, *106*, 5058.
(29) Norman, G. E.; Filinov, V. S. *High Temp.* **1969**, *7*, 216.
(30) Buss, E.; Heuchel, M. *J. Chem. Soc., Faraday Trans.* **1997**, *93*, 1621.
(31) Goodbody, S. J.; Watanabe, K.; MacGowan, D.; Walton, J. P. R.; Quirke, N. *J. Chem. Soc., Faraday Trans.* **1991**, *87*, 1951.
(32) Heuchel, M.; Snurr, R. Q.; Buss, E. *Langmuir* **1997**, *13*, 6795.
(33) Laaksonen, L. *gOpenMol*, 2.0 ed.; CRC, Finnish IT centre for science: Espoo, Finland, 2001.

NL0341281